Prog. Theor. Exp. Phys. **2024** 103B06 (16 pages)
DOI: 10.1093/ptep/ptae152

Imprinting New Physics by Using Angular Profiles of the Flavor-Changing-Neutral-Current Process $B_c \to D_s^* (\to D_s\pi)\ell^+\ell^-$

Hira Waseem and Abdul Hafeez[*]

Department of Physics, Quaid-i-Azam University, Islamabad Capital Territory, 15320, Pakistan

*Email: abdulhafeez@phys.qau.edu.pk

Received September 3, 2024; Revised October 8, 2024; Accepted October 10, 2024; Published October 11, 2024

The decays governed by the flavor-changing-neutral-current (FCNC) transitions, such as $b \to s\ell^+\ell^-$, provide an important tool to test the physics in and beyond the Standard Model (SM). This work focuses on investigating the FCNC process $B_c \to D_s^* (\to D_s\pi)\ell^+\ell^-(\ell = e, \mu, \tau)$. Being an exclusive process, the initial and final state meson matrix elements involve the form factors, which are nonperturbative quantities and need to be calculated using specific models. By using the form factors calculated in the covariant light-front quark model, we analyze the branching fractions and angular observables such as the forward-backward asymmetry $A_{\rm FB}$, polarization fractions (longitudinal and transverse) $F_{L(T)}$, CP asymmetry coefficients A_i, and CP-averaged angular coefficients S_i, both in the SM and in some new physics (NP) scenarios. Some of these physical observables are a potential source of finding the physics beyond the SM and help us to distinguish various NP scenarios.

Subject Index B51

1. Introduction

Several results from the last few decades have some (1–3)σ disagreement with the Standard Model (SM) results, and the flavor-changing-neutral-current (FCNC) processes involving $b \to s$ are the pertinent ones here. The Glashow–Iliopoulos–Maiani (GIM) mechanism allows these transitions at loop level in the SM, and due to their strong suppression within the SM, exclusive and inclusive $b \to s\ell^+\ell^-$ decays are potential probes of short-distance physics. Also, their sparkling sensitivity to new physics (NP) particles makes them a harbinger to study the NP indirectly [1]. In 2013, the observation of tension by the Large Hadron Collider beauty led to the assumption of the presence of NP [2]. In 2014, another dilemma was confronted within the SM, namely, the suppression of the ratio R_K for $B \to K\ell^+\ell^-(\ell = e, \mu)$ at low dilepton invariant mass and for the consistent description of these anomalies resulted in the presence of NP [3]. Additionally, the calculated value of the branching ratio of $B_{(s)} \to \phi\mu^{(+)}\mu^{(-)}$ [4] was small compared to the SM observations [5,6].

One of the most optimized observables ($\mathcal{P}_5$) in $B \to K^*\mu^+\mu^-$ decay has shown a mismatch with the SM predictions [7,8]. The Yukawa sector of the SM was also scrutinized by measuring the Lepton Flavor Universality (LFU) ratio $\mathcal{R}_{K^{(*)}} \equiv \frac{\mathcal{B}(B\to K^{(*)}\mu^+\mu^-)}{\mathcal{B}(B\to K^{(*)}e^+e^-)}$ in various bins of the transferred square momentum, i.e. $q^2 = (p_{\ell^+} + p_{\ell^-})^2$ and almost 3σ deviations from the SM predictions were recorded at the LHCb [9–11]. However, the situation

Funded by SCOAP³

changed after the latest measurements of LHCb in the low and central q^2 region [12,13], bringing the LFU ratio into agreement with the SM predictions. Motivated by these tensions, several theoretical studies were performed for the complementary exclusive decays $B \to \left(K_1(1270, 1430), K_2^*(1430), f_2'(1525)\right)\ell^+\ell^-$ in the SM and various NP models [14–22]. The semileptonic decays involving tauons initially received less attention than the muon and electron in the final state. This situation has now changed, and after experimental improvements, these decays are in the limelight now [23–27]. Theoretically, to scrutinize the various NP models, the semileptonic B-meson decays occurring through the FCNC transition $b \to (s, d)\tau^+\tau^-$ have been investigated in several studies, see e.g. Refs. [28–36]. In contrast to the ordinary B-meson decays, the B_c decay may proceed through the weak decay of either of its heavy constituents, i.e. b or c, and the other will play the role of spectator. It can also decay virtually to the W^+ boson, and its lifetime is almost one-third of that of the B^0, B^+ [37–39]. Recently, using the $9\,fb^{-1}$ data of the proton–proton collision at the LHC, the LHCb has performed searches for $B_c^+ \to D_s^+\mu^+\mu^-$ decay, but these have not observed any significant signal in the nonresonant dimuonic mode. The upper limits on $\frac{f^c}{f^u} \times \mathcal{B}\left(B_c^+ \to D_s^+\mu^+\mu^-\right) < 9.6 \times 10^{-8}$ are set with 95%. Here, f^c and f^u are the fragmentation fractions of a B meson having c and u quarks [40]. As D_s^* needs to be rebuilt from the D_s meson experimentally, it will be a little tough to measure $B_c \to D_s^*\ell^+\ell^-$ but the situation can be made better with an upgrade in the high luminosity of the LHCb in future.

On theoretical fronts, the semileptonic $B_c \to D_s^*$ decay was studied in several approaches, e.g. the light-front quark model (LFQM) [41], the perturbative quantum chromodynamics (pQCD) approach [42], the QCD sum rule [43,44], the constituent quark model (CQM) [41], etc. In the SM, the branching ratio for the electron and muon mode is calculated to be of the order of 10^{-8} while for the tau it is 10^{-9}; in particular, various physical observables of $B_c \to D_s^*\mu^+\mu^-$ decay have been calculated in the SM and beyond in Refs. [45–47]. Including the τ leptons in the final state, $B_c \to D_s^*\ell^+\ell^-$ has been studied in Ref. [48], where Li and Liu have calculated the form factors in the covariant LFQM approach. Also, the full calculation of the angular distribution of the quasi-fourfold distribution $B_c \to D_s^*(D\pi)\ell^+\ell^-$ has been done to study various physical observables.

As a follow-up of the study presented in Ref. [48], using their form factors, we will first analyze the branching fractions and angular observables such as the forward-backward asymmetry A_{FB}, polarization fractions $F_{L(T)}$, and CP-averaged angular observables (S_i, A_i) both in the SM and beyond. For the physics beyond the SM (BSM), we used the latest model-independent global fit to $b \to s\ell^+\ell^-$ observables which include the latest measurements by the LHCb of observables of $B_s \to \mu^+\mu^-$, $B_s \to \phi\mu^+\mu^-$, R_{K,K_S}, and R_{K^*} and added the 254 observables to find the pattern of the NP that successfully explains the data [49]. We hope our findings will complement the various asymmetries observed in FCNC decays.

The structure of this paper is organized as follows: Following the introductory section, we present the angular distributions of the quasi-four body decays $B_c \to D_s^*(\to D_s\pi)\ell^+\ell^-$ in Sections 2 and 3. In Section 4, we introduce the form factors derived by the covariant LFQM in Ref. [48]. Section 5 presents numerical results for several observables in the SM and next-generation physics using NP models 50. Finally, this paper ends with an outline.

2. Effective Hamiltonian in SM and BSM

The low-energy effective Hamiltonian for $b \to s\ell^+\ell^-$ in the model-independent way is written as [51],

$$\mathcal{H}_{\text{eff}} = -\frac{4G_F}{\sqrt{2}}\left[\lambda_u\left(C_1\left(\mathcal{O}_1^u - \mathcal{O}_1^c\right) + C_2\left(\mathcal{O}_2^u - \mathcal{O}_2^c\right)\right) + \lambda_t \sum_{i\in J} C_i\mathcal{O}_i\right], \quad (1)$$

where λ_q denotes $V_{qb}V_{qs^*}$ and $J = \left(1_c, 2_c, 3...8, 7^{(\prime)}, 9l^{(\prime)}, 10l^{(\prime)},\ Sl^{(\prime)}, Pl^{(\prime)}, Tl^{(\prime)}\right)$. V_{ij} stands for the Cabibbo–Kobayashi–Maskawa (CKM) matrix elements and the Fermi constant is represented by $G_F = 1.16637 \times 10^{-5}$ GeV^{-2}. $C_i(\mu)$ are the Wilson coefficients that tell us about the strength of the interaction and $\mathcal{O}_i$ are the four fermion operators while μ is the renormalization scale. Particularly, $\mathcal{O}_{1,2}$ are the current-current operators, $\mathcal{O}_{3-6}$ are the penguin operators, $\mathcal{O}_{7,8}$ are the electromagnetic operators, and $\mathcal{O}_{9,10}$ are the semileptonic operators and their corresponding Wilson coefficients describe the coupling strength between the respective quarks and charged leptons at the factorization scale $\mu = m_b$. Short-distance physics is encoded in Wilson coefficients of higher-dimension operators. In the SM, the effective Hamiltonian contains ten operators with specific chiralities due to the V-A structure of weak interactions where the heavy degrees of freedom are integrated out, and we are left with only the operators set, describing the long-distance physics [52].

Here, the effective Hamiltonian used has the following form:

$$\mathcal{H}_{\text{eff}}\left(b \to s\ell^+\ell^-\right) = -\frac{4G_F}{\sqrt{2}}V_{tb}V_{ts}^*\frac{\alpha_e}{4\pi}\left[\bar{s}\left(C_9^{\text{eff}}(q^2,\mu)\gamma^\mu P_L - \frac{2m_b}{q^2}C_7^{\text{eff}}(\mu)i\sigma^{\mu\nu}q_\nu P_R\right)b(\bar{\ell}\gamma_\mu\ell)\right.$$
$$\left. + C_{10}(\mu)\left(\bar{s}\gamma^\mu P_L b\right)\left(\bar{\ell}\gamma^\mu\gamma_5\ell\right)\right], \quad (2)$$

where P_L and P_R stand for the left and right projection operators, respectively, $\sigma^{\mu\nu} = i(\gamma^\mu\gamma^\nu - \gamma^\nu\gamma^\mu)/2$, and α_e stands for the electromagnetic coupling which is $\frac{1}{137}$. The operators have the form,

$$\mathcal{O}_7 = \frac{e}{16\pi^2}m_b\left(\bar{s}\sigma_{\mu\nu}P_R b\right)F^{\mu\nu},$$
$$\mathcal{O}_9 = \frac{e^2}{16\pi^2}\left(\bar{s}\gamma_\mu P_L b\right)\left(\bar{l}\gamma^\mu l\right),$$
$$\mathcal{O}_{10} = \frac{e^2}{16\pi^2}\left(\bar{s}\gamma_\mu\gamma_5 P_L b\right)\left(\bar{l}\gamma^\mu l\right). \quad (3)$$

Here, operator $\mathcal{O}_7$ represents the interaction between photons and quarks whereas $\mathcal{O}_{9,10}$ represents the interaction between quarks and leptons, respectively. C_7^{eff} and C_9^{eff} are represented by

$$C_7^{\text{eff}}(\mu) = C_7(\mu) + C'_{b\to s\gamma}(\mu)$$
$$C_9^{\text{eff}}(q^2,\mu) = C_9(\mu) + C_{9,\text{pert}}(q^2,\mu) + C_{9,c\bar{c}}(q^2,\mu), \quad (4)$$

where $C'_{b\to s\gamma}(\mu)$ results from the following interaction: $b \to sc\bar{c} \to s\gamma$ [53]. $C_{9,\text{pert}}(q^2,\mu)$ and $C_{9,c\bar{c}}(q^2,\mu)$ represent the short- and long-distance contributions, respectively, as $C_{9,\text{pert}}(q^2,\mu)$ results from the one-loop matrix element of the four fermi quark operators $\mathcal{O}_{1-6}$. It can be calculated at leading order within perturbation theory while $C_{9,c\bar{c}}(q^2,\mu)$ relies upon the external hadron states. Putting everything together [54]:

$$C'_{b\to s\gamma}(\mu) = i\alpha_s \left[\frac{2}{9}\eta^{\frac{14}{23}} \left(\frac{y_t\left(y_t^2 - 5y_t - 2\right)}{8\left(y_t - 1\right)^3} + \frac{3y_t^2 \log y_t}{4\left(y_t - 1\right)^4} - 0.1687 \right) - 0.03 \times C_2(\mu) \right], \tag{5}$$

with $y_t = \frac{m_t^2}{m_W^2}$, $\eta = \frac{\alpha_s(m_W)}{\alpha_s(\mu)}$, and the mass scale $\mu = m_b$.

$$\begin{aligned} C_{9,\mathrm{pert}}(\hat{s}, \mu) = {} & 0.124\omega(\hat{s}) + \mathrm{g}(\hat{m}_c, \hat{s})\, C_\mu + \lambda_\mu \Big[\mathrm{g}(\hat{m}_c, \hat{s}) - \mathrm{g}(0, \hat{s}) \Big] \\ & \times \left(3C_1(\mu) + C_2(\mu)\right) - \frac{1}{2}\mathrm{g}(0, \hat{s})\left(C_3(\mu) + 3C_4(\mu)\right) \\ & - \frac{1}{2}\mathrm{g}(1, \hat{s})\left(4C_3(\mu) + 4C_4(\mu) + 3C_5(\mu) + C_6(\mu)\right) \\ & + \frac{2}{3}C_3(\mu) + \frac{2}{9}C_4(\mu) + \frac{2}{3}C_5(\mu) + \frac{2}{9}C_6(\mu), \end{aligned} \tag{6}$$

where $\hat{s} = \frac{q^2}{m_b^2}$, $\hat{m}_c = \frac{m_c}{m_b}$, and $C(\mu) = 3C_{1,3,5}(\mu) + C_{2,4,6}(\mu)$. The Wilson coefficients are chosen at $\mu = m_b$ and their numerical values read as $C_1 = -0.226$, $C_2 = 1.096$, $C_3 = 0.01$, $C_4 = -0.024$, $C_5 = 0.007$, $C_6 = -0.028$, $C_7 = -0.305$, $C_8 = -0.15$, $C_9 = 4.186$, $C_{10} = -4.559$ [55]. In the Wolfenstein representation, the λ_μ has the following form [56]:

$$\lambda_\mu \approx -\lambda^2(\rho - i\eta), \tag{7}$$

and $\lambda = 0.22500 \pm 0.00067$. Here the function $\omega(\hat{s})$ is defined as [57]:

$$\begin{aligned} \omega(\hat{s}) = {} & -\frac{2}{9}\pi^2 + \frac{4}{3}\int_0^{\hat{s}} \frac{\log(1-u)}{u} du - \frac{2}{3}\log\hat{s}\log(1-\hat{s}) - \frac{5+4\hat{s}}{3(1+2\hat{s})}\log(1-\hat{s}) \\ & - \frac{2\hat{s}(1+\hat{s})(1-2\hat{s})}{3(1-\hat{s})^2(1+2\hat{s})}\log\hat{s} + \frac{5+9\hat{s}-6\hat{s}^2}{6(1-\hat{s})(1+2\hat{s})}, \end{aligned} \tag{8}$$

and the functions $\mathrm{g}(z, \hat{s})$have the form [58,59]:

$$\begin{aligned} & \mathrm{g}(z, \hat{s}) = -\frac{8}{9}\log(z) + \frac{8}{27} + \frac{4}{9}y - \frac{2}{9}(2+y)\sqrt{|1-y|} \times \left\{ \log\left| \frac{1+\sqrt{1-y}}{-1+\sqrt{1-y}} \right| - i\pi \right\} \quad \text{for} \quad y \equiv \frac{4z^2}{\hat{s}} < 1 \\ & \mathrm{g}(z, \hat{s}) = -\frac{8}{9}\log(z) + \frac{8}{27} + \frac{4}{9}y - \frac{2}{9}(2+y)\sqrt{|1-y|} \times 2\arctan\frac{1}{\sqrt{y-1}} \quad \text{for} \quad y \equiv \frac{4z^2}{\hat{s}} > 1, \end{aligned} \tag{9}$$

which for $q^2 = 0$ becomes:

$$g(0, \hat{s}) = \frac{8}{27} - \frac{8}{9}\log\left(\frac{m_b}{\mu}\right) - \frac{4}{9}\log\hat{s} + \frac{4}{9}i\pi. \tag{10}$$

The $C_{9,c\bar{c}(q^2,\mu)}$ has the contributions from the intermediate light vector mesons and vector charmonium states [60]:

$$\begin{aligned} C_{9,c\bar{c}(q^2,\mu)} = -\frac{3\pi}{\alpha_e^2} \Bigg[& C(\mu) \sum_{V_i = J/\psi, \psi(2S), \ldots} \frac{m_{V_i}\mathcal{B}\left(V_i \to l^+l^-\right)\Gamma_{V_i}}{q^2 - m_{V_i}^2 + i m_{V_i}\Gamma_{V_i}} - \lambda_u \mathrm{g}(0, \hat{s})\Big(3C_1(\mu) + C_2(\mu)\Big) \\ & \sum_{V_j = \rho, \omega, \ldots} \frac{m_{V_j}\mathcal{B}(V_j \to l^+l^-)\Gamma_{v_j}}{q^2 - m_{V_j}^2 + i m_{V_j}\Gamma_{V_j}} \Bigg], \end{aligned} \tag{11}$$

where m_{V_i} and Γ_{V_i} represent the mass in GeV and the total decay rate of the particular resonance particle in MeV, respectively. These values are taken from the Particle Data Group [61] and represented in Table 1.

Table 1. Properties of resonances and the values of input parameters involved in effective Wilson coefficients [48].

V_i	m_{V_i}	Γ_{V_i}	$\mathcal{B}(V_i \to \ell^+\ell^-) \times 10^{-5}$
ρ	0.775	149	4.635
ω	0.783	8.68	7.380
ϕ	1.019	4.249	$2.915 \times 10^{+1}$
J/ψ	3.097	0.093	$5.966 \times 10^{+3}$
$\psi(2S)$	3.686	0.294	$7.965 \times 10^{+2}$
$\psi_{(3770)}$	3.774	27.2	9.6×10^{-1}
$\psi_{(4040)}$	4.039	80	$1.07 \times 10^{+1}$
$\psi_{(4160)}$	4.191	70	6.9×10^{-1}

3. Angular distributions and the observables

By definition of the transition probability amplitude,

$$\langle D_s^*(p^{(2)})|\bar{s}\gamma_\mu b|B_c(p^{(1)})\rangle = \epsilon_{\mu\nu\alpha\beta}\epsilon^{*\nu}P^\alpha q^\beta g(q^2),$$
$$\langle D_s^*(p^{(2)})|\bar{s}\gamma_\mu\gamma_5 b|B_c(p^{(1)})\rangle = -i\left[\epsilon_\mu^* f\left(q^2\right) + \epsilon^*.P\left(P_\mu a_+\left(q^2\right) + q_\mu a_-\left(q^2\right)\right)\right], \tag{12}$$

where $P_\mu = p_\mu^{(1)} + p_\mu^{(2)}$ and $q_\mu = p_\mu^{(1)} - p_\mu^{(2)}$. Also, ϵ represents the polarization vector of the D_s^* meson. The expression of amplitudes in the Bauer–Stech–Wirbel (BSW) form [62] is as follows:

$$\langle D_s^*(p^{(2)})|\bar{s}\gamma_\mu b|B_c(p^{(1)})\rangle = -\frac{1}{m_1+m_2}\epsilon_{\mu\nu\alpha\beta}\epsilon^{*\nu}P^\alpha q^\beta V(q^2),$$
$$\langle D_s^*(p^{(2)})|\bar{s}\gamma_\mu\gamma_5 b|B_c(p^{(1)})\rangle = i\left[(m_1+m_2)\epsilon_\mu^* A_1\left(q^2\right) - \frac{\epsilon^*.P}{m_1+m_2}P_\mu A_2\left(q^2\right)\right.$$
$$\left. -2m_2\frac{\epsilon^*.P}{q^2}q_\mu\left[A_3\left(q^2\right) - A_0\left(q^2\right)\right]\right], \tag{13}$$

where the mass of the B_c meson is m_1, while the mass of the D_s^* meson is m_2. Additionally, tensor current amplitude is defined as [63]:

$$\langle D_s^*(p^{(2)})|\bar{s}i\sigma^{\mu\nu}q_\nu b|B_c(p^{(1)})\rangle = T_1(q^2)\epsilon_{\alpha\beta\mu\nu}\epsilon_\nu^* P^\alpha q^\beta,$$
$$\langle D_s^*(p^{(2)})|\bar{s}i\sigma^{\mu\nu}q_\nu\gamma 5b|B_c(p^{(1)})\rangle = iT_2\left(q^2\right)\left[\left(m_1^2-m_2^2\right)\epsilon_\mu^* - \epsilon^*.qP_\mu\right]$$
$$+iT_3\left(q^2\right)\epsilon^*.q\left[q_\mu - \frac{q^2P_\mu}{m_1^2-m_2^2}\right]. \tag{14}$$

Here, $V(q^2)$, $A_1\left(q^2\right)$, $A_2\left(q^2\right)$, $A_3\left(q^2\right)$, $A_0\left(q^2\right)$, $T_1\left(q^2\right)$, $T_2\left(q^2\right)$, $T_3\left(q^2\right)$ are the form factors [64–66]. By using the above definitions of the matrix elements, the invariant amplitude is written in the following form [48]:

$$\mathcal{M}(s_{l^+}, s_{l^-}) = \langle D_s\pi;\, l^+(s_{l^+})l^-(s_{l^-})|\mathcal{H}_{\text{eff}}|B_c\rangle$$
$$= \sum_{s_v}\frac{I}{k^2-m_{D_s^*}^2}\mathcal{M}_{D_s^*\to D_s\pi}\left(s_V\right)\langle D_s^*\left(s_V\right)l^+\left(s_{l^+}\right)l^-\left(s_{l^-}\right)|\mathcal{H}_{\text{eff}}|B_c\rangle, \tag{15}$$

where $\mathcal{M}_{D_s^*\to D_s\pi}$ is

$$\mathcal{M}_{D_s^*\to D_s\pi} = -ig_{D_s^*D_s}\epsilon^\mu p_\mu^\pi. \tag{16}$$

Table 2. The helicity combinations that correspond to different angular distributions.

i	$J_i\left(q^2\right)$	$f_i\left(\theta,\theta_l,\phi\right)$
1s	$\left(\frac{3}{4}-\hat{m}_l^2\right)\left(\left\|\mathcal{A}_L^{\parallel}\right\|^2+\left\|\mathcal{A}_L^{\perp}\right\|^2+\left\|\mathcal{A}_R^{\perp}\right\|^2+\left\|\mathcal{A}_R^{\parallel}\right\|^2\right)+ 4\hat{m}_l^2\mathrm{Re}\left[\mathcal{A}_L^{\perp}\mathcal{A}_{R^*}^{\perp}+\mathcal{A}_L^{\parallel}\mathcal{A}_{R^*}^{\parallel}\right]$	$\sin^2\theta$
1c	$\left\|\mathcal{A}_L^0\right\|^2+\left\|\mathcal{A}_R^0\right\|^2+4\hat{m}_l^2\left(\left\|\mathcal{A}^t\right\|^2+2\mathrm{Re}\left[\mathcal{A}_L^0\mathcal{A}_{R^*}^0\right]\right)$	$\cos^2\theta$
2s	$\beta_l^2\left(\left\|\mathcal{A}_L^{\parallel}\right\|^2-\left\|\mathcal{A}_L^{\perp}\right\|^2+\left\|\mathcal{A}_R^{\parallel}\right\|^2+\left\|\mathcal{A}_R^{\perp}\right\|^2\right)\Big/4$	$\sin^2\theta\cos 2\theta_l$
2c	$-\beta_l^2\left(\left\|\mathcal{A}_L^0\right\|^2+\left\|\mathcal{A}_R^0\right\|^2\right)$	$\cos^2\theta\cos 2\theta_l$
3	$\beta_l^2\left(\left\|\mathcal{A}_L^{\perp}\right\|^2-\left\|\mathcal{A}_L^{\parallel}\right\|^2+\left\|\mathcal{A}_R^{\perp}\right\|^2-\left\|\mathcal{A}_R^{\parallel}\right\|^2\right)\Big/2$	$\sin^2\theta\sin^2\theta_l\cos 2\phi$
4	$\beta_l^2\mathrm{Re}\left[\mathcal{A}_L^0\mathcal{A}_{L^*}^{\parallel}+\mathcal{A}_R^0\mathcal{A}_{R^*}^{\parallel}\right]\Big/\sqrt{2}$	$\sin 2\theta\sin 2\theta_l\cos\phi$
5	$\sqrt{2}\beta_l\mathrm{Re}\left[\mathcal{A}_L^0\mathcal{A}_{L^*}^{\perp}-\mathcal{A}_R^0\mathcal{A}_{R^*}^{\perp}\right]$	$\sin 2\theta\sin\theta_l\cos\phi$
6s	$2\beta_l\mathrm{Re}\left[\mathcal{A}_L^{\parallel}\mathcal{A}_{L^*}^{\perp}-\mathcal{A}_R^{\parallel}\mathcal{A}_{R^*}^{\perp}\right]$	$\sin^2\theta\cos\theta_l$
7	$\sqrt{2}\beta_l\mathrm{Im}\left[\mathcal{A}_L^0\mathcal{A}_{L^*}^{\parallel}-\mathcal{A}_R^0\mathcal{A}_{R^*}^{\parallel}\right]$	$\sin 2\theta\sin\theta_l\sin\phi$
8	$\beta_l^2\mathrm{Im}\left[\mathcal{A}_L^0\mathcal{A}_{L^*}^{\perp}-\mathcal{A}_R^0\mathcal{A}_{R^*}^{\perp}\right]\Big/\sqrt{2}$	$\sin 2\theta\sin 2\theta_l\sin\phi$
9	$\beta_l^2\mathrm{Im}\left[\mathcal{A}_{L^*}^{\parallel}\mathcal{A}_L^{\perp}+\mathcal{A}_{R^*}^{\parallel}\mathcal{A}_R^{\perp}\right]$	$\sin^2\theta\sin^2\theta_l\sin 2\phi$

Using the effective Lagrangian approach for the calculation, the amplitude has the following form:

$$\mathcal{M}\left(s_{l^+},s_{l^-}\right)=\sum_{s_v}\frac{I}{k^2-m_{D_s^*}^2}\mathcal{M}_{D_s^*\to D_s\pi}\left(s_V\right)\Bigg[C_9^{\mathrm{eff}}H^{V-A}\left(s_V,t\right)L^V\left(s_{l^+},s_{l^-},t\right)-\frac{2m_b}{q^2}C_7^{\mathrm{eff}}H^{T+T5}\left(s_V,t\right)$$
$$L^V\left(s_{l^+},s_{l^-},t\right)+C_{10}H^{V-A}\left(s_V,t\right)L^A\left(s_{l^+},s_{l^-},t\right)-\sum_{\lambda=0,\pm}\Bigg(C_9^{\mathrm{eff}}H^{V-A}\left(s_V,\lambda\right)L^V\left(s_{l^+},s_{l^-},\lambda\right)$$
$$-\frac{2m_b}{q^2}C_7^{\mathrm{eff}}H^{T+T5}\left(s_V,\lambda\right)L^V\left(s_{l^+},s_{l^-},\lambda\right)+C_{10}H^{V-A}\left(s_V,\lambda\right)L^A\left(s_{l^+},s_{l^-},\lambda\right)\Bigg)\Bigg]. \tag{17}$$

In this equation, $N=\frac{4G_F\alpha_e V_{tb}V_{ts}^*}{4\pi\sqrt{2}}$ and a factor of $\frac{1}{2}$ comes from the right- and left-hand projection operators mentioned in Eq. (2). Helicity amplitudes are mentioned in Ref. [67]. Finally, by using the effective Hamiltonian as mentioned in Eq. (2), the simplified form of angular distribution as deduced in Ref. [68] is

$$\frac{d^4\Gamma}{dq^2\, dc_\theta\, dc_{\theta_l}\, d\phi}=\frac{9}{32\pi}\sum_i J_i(q^2)f_i(\theta,\theta_l,\phi), \tag{18}$$

where c_θ represents $\cos\theta$. Each of these is mentioned in Table 2. In the given scenario, the angle θ represents the deviation between the direction of pion emission and the $-\hat{z}$ rest frame direction of the D_s^* meson. Similarly, θ_l denotes the angle formed by the ℓ^- particle with the $+\hat{z}$ rest frame direction of the $\ell^+\ell^-$ pair, and ϕ is the angle made between the planes of the decay as presented in Fig. 1.

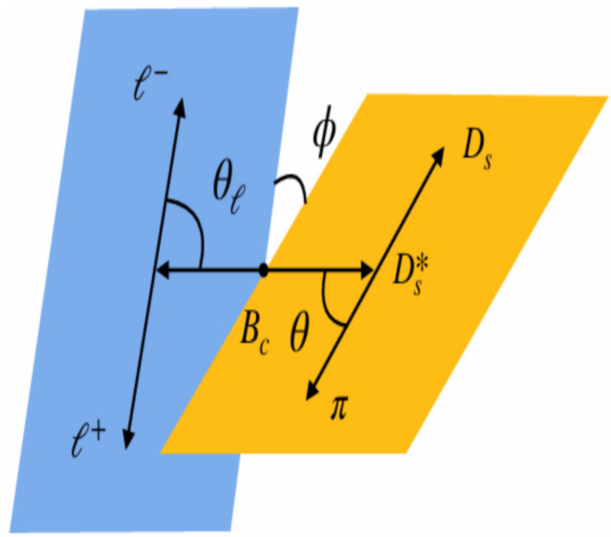

Fig. 1. Scattering kinematics of quasi-fourfold distribution [48].

The corresponding amplitudes for the particular polarizations have the parametrized form and are the functions of q^2 [69].

$$\mathcal{A}^{\perp}_{L,R}\left(q^2\right) = -N_l\sqrt{2N_{D_s^*}}\sqrt{\lambda\left(m_1^2, m_2^2, q^2\right)}\left\{\left(C_9^{\text{eff}} \mp C_{10}\right)\frac{V\left(q^2\right)}{m_1+m_2} + 2\hat{m}_b C_7^{\text{eff}} T_1\left(q^2\right)\right\},$$

$$\mathcal{A}^{\parallel}_{L,R}\left(q^2\right) = N_l\sqrt{2N_{D_s^*}}\left\{\left(C_9^{\text{eff}} \mp C_{10}\right)(m_1+m_2)A_1\left(q^2\right) + 2\hat{m}_b C_7^{\text{eff}}\left(m_1^2 - m_2^2\right)T_2\left(q^2\right)\right\},$$

$$\mathcal{A}^{0}_{L,R}\left(q^2\right) = \frac{N_l\sqrt{2N_{D_s^*}}}{2m_2\sqrt{q^2}}\left\{\left(C_9^{\text{eff}} \mp C_{10}\right)\left[\left(m_1^2 - m_2^2 - q^2\right)(m_1+m_2)A_1\left(q^2\right) - \frac{\lambda\left(m_1^2, m_2^2, q^2\right)}{m_1+m_2}A_2\left(q^2\right)\right]\right.$$
$$\left. + 2m_b C_7^{\text{eff}}\left[\left(m_1^2 + 3m_2^2 - q^2\right)T_2\left(q^2\right) - \frac{\lambda\left(m_1^2, m_2^2, q^2\right)}{m_1^2 - m_2^2}T_3\left(q^2\right)\right]\right\},$$

$$\mathcal{A}^{t}(q^2) = 2N_l\sqrt{2N_{D_s^*}}\frac{\sqrt{\lambda\left(m_1^2, m_2^2, q^2\right)}}{\sqrt{q^2}}C_{10}A_0\left(q^2\right), \tag{19}$$

where

$$N_l = \frac{i\alpha_e G_F V_{tb}V_{ts}^*}{4\ pi\sqrt{2}},$$

$$N_{D_s^*} = \frac{8\sqrt{\lambda}q^2}{3\times 256\pi^3 m_1^3}\sqrt{1 - \frac{4m_l^2}{q^2}}\mathcal{B}\left(D_s^* \to D_s\pi\right). \tag{20}$$

Regarding the conjugated CP mode, $B_c^+ \to D_s^{*+}(\to D_s\pi)\,l^+l^-$ weak phase conjugations of the CKM elements lead to

$$\frac{d^4\bar{\Gamma}}{dq^2\ dc_\theta\ dc_{\theta_l}\ d\phi} = \frac{9}{32\pi}\sum_i \bar{J}_i(q^2)f_i\left(\theta, \theta_l, \phi\right) \tag{21}$$

with the substitutions as $J_{1(c,s),2(c,s),3,4,7} \to \bar{J}_{1(c,s),2(c,s),3,4,7}$ and $J_{5,6s,8,9} \to -\bar{J}_{5,6s,8,9}$. By doing integration over the angles in the domain $\theta \in [0, \pi]$, $\theta_l \in [0, \pi]$, and $\phi \in [0, 2\pi]$, the differential width becomes only the function of q^2, so,

$$\frac{d\Gamma}{dq^2} = \frac{1}{4}\left(3J_{1c} + 6J_{1s} - J_{2c} - 2J_{2s}\right). \tag{22}$$

A similar expression results for the conjugated mode of the transition so that the CP-average differential decay width can be written as,

$$\frac{d\Gamma}{dq^2} = \frac{1}{2}\left(\frac{d\Gamma}{dq^2} + \frac{d\bar{\Gamma}}{dq^2}\right). \tag{23}$$

To disentangle the CP-conserving and -violating effects, CP (angular S_i and asymmetry angular A_i) coefficients are defined as

$$S_i = \frac{J_i + \bar{J}_i}{d\left(\Gamma + \bar{\Gamma}\right)/dq^2},$$
$$A_i = \frac{J_i - \bar{J}_i}{d\left(\Gamma + \bar{\Gamma}\right)/dq^2}, \tag{24}$$

where J_i's are the angular coefficients defined in Ref. [48]. Several observables can be constructed from these J_i coefficients, and these quasi-four body processes are sensitive to NP. Other physical observables can be calculated such as forward-backward asymmetry A_{FB}, and longitudinal and transverse polarization fractions $F_{L(T)}$ of D_s^* mesons. This we have done in the next few sections.

4. Observables and form factors

The Standard relation for the CP asymmetry lepton forward-backward asymmetry is,

$$A_{\mathrm{CP}}^{\mathrm{FB}}\left(q^2\right) = \frac{1}{d\left(\Gamma + \bar{\Gamma}\right)/dq^2} \times \int_{-1}^{1} d\cos\theta_l \int_{-1}^{1} d\cos\theta \int_{0}^{2\pi} d\phi \frac{d^4\left(\Gamma + \bar{\Gamma}\right)}{dq^2 d\cos\theta d\cos\theta_l d\phi} = \frac{3}{4}A_6, \tag{25}$$

whereas the CP-averaged forward-backward asymmetry is,

$$A_{\mathrm{FB}}\left(q^2\right) = \frac{3}{4}S_6. \tag{26}$$

The polarizations are defined as

$$F_L = \frac{1}{4}\left(3S_{1c} - S_{2c}\right),$$
$$F_T = \frac{1}{2}\left(3S_{1s} - S_{2s}\right). \tag{27}$$

We also focus on the LFU ratios as these are important to trace out NP, i.e.

$$R^{\mu e} = \frac{\int_{4\mu^2}^{(m_1-m_2)^2} \frac{d\Gamma\left(B_c \to D_s^*(\to D_s\pi)\mu^+\mu^-\right)}{dq^2} dq^2}{\int_{4\mu^2}^{(m_1-m_2)^2} \frac{d\Gamma\left(B_c \to D_s^*(\to D_s\pi)e^+e^-\right)}{dq^2} dq^2},$$
$$R^{\tau\mu} = \frac{\int_{4\mu^2}^{(m_1-m_2)^2} \frac{d\Gamma\left(B_c \to D_s^*(\to D_s\pi)\tau^+\tau^-\right)}{dq^2} dq^2}{\int_{4\mu^2}^{(m_1-m_2)^2} \frac{d\Gamma\left(B_c \to D_s^*(\to D_s\pi)\mu^+\mu^-\right)}{dq^2} dq^2}. \tag{28}$$

The form factors used in this work are taken from Ref. [48], in which entities are derived using the covariant LFQM, which is considered best for exploring mesons and baryons. This model requires initial mesons to be on the shell compared to conventional LFQM [70,71]. They use the z-series parametrization form for the form factors to perform analytical continuation [72,73].

$$\mathrm{F}(q^2) = \frac{\mathrm{F}(0)}{1-\frac{q^2}{m^2_{\mathrm{pole}}}}\Bigg\{1 + a_1\left[\left(\mathrm{z}(q^2) - \mathrm{z}(0)\right) - \frac{1}{3}\left(\mathrm{z}\left(q^2\right)^3 - \mathrm{z}(0)^3\right)\right]$$
$$+ a_2\left[\left(\mathrm{z}\left(q^2\right)^2 - \mathrm{z}(0)^2\right) + \frac{2}{3}\left(\mathrm{z}\left(q^2\right)^3 - \mathrm{z}(0)^3\right)\right]\Bigg\}, \tag{29}$$

where a_i are the fitting parameters in space-like region $q^2 < 0$ and $\mathrm{z}\left(q^2\right)$ is defined as,

$$\mathrm{z}\left(q^2\right) = \frac{\sqrt{(m_1+m_2)^2 - q^2} - \sqrt{(m_1+m_2)^2 - (m_1-m_2)^2}}{\sqrt{(m_1+m_2)^2 - q^2} + \sqrt{(m_1+m_2)^2 - (m_1-m_2)^2}}. \tag{30}$$

The values of free parameters a_i and all the form factors at $q^2 = 0$ are as given in Ref. [48]. Form factors for $B_c \to D_s^*$ are calculated by using different approaches in Refs. [74–76] but here only central values are taken in the present analysis.

5. New model benchmarks and parameters

For the SM Wilson coefficients we use, $C_7^{\mathrm{SM}} = -0.305$, $C_9^{\mathrm{SM}} = 4.186$, $C_{10}^{\mathrm{SM}} = -4.559$ which are found at $\mu = m_b$. By omitting the CKM unitarity, we can determine the CKM elements $V_{ts}V_{tb}^*$ [77]:

$$V_{ts}V_{tb}^* = -V_{cb}\left[1 - \frac{\lambda^2}{2}\left(1 - 2\bar{\rho} + 2i\bar{\eta}\right)\right] + O\left(\lambda^6\right), \tag{31}$$

so, we took

$$|V_{tb}V_{ts}^*| = (41.4 \pm 0.5) \times 10^{-3}. \tag{32}$$

The lifetime of B_c meson $\tau_{B_c} = 0.510$ ps is taken from the Particle Data Group, and the branching fraction $\mathcal{B}\left(D_s^* \to D_s\pi\right) = 5 \times 10^{-2}$. Finally, we found the CP-averaged differential branching ratios as calculated within the $q^2\left(\mathrm{GeV}^2\right)$ bin [1.1, 6.0] and other physical observables in the different $q^2\left(\mathrm{GeV}^2\right)$ bins [1.1, 6.0], [6.0, 8.0], [11, 12.5], and [15, 17] for all the three generations of leptons. The branching fractions of electron and muon are of the order of 10^{-8} magnitude whereas that for tau in the bin [15, 17] can reach up to 10^{-9}. $R^{\mu e}$ is consistent with the SM prediction, i.e. 1.00, and $R^{\tau\mu} = 0.3801$. In the region [1.1, 6.0] GeV^2, the branching fraction for electron and muon is

$$\mathcal{B}\left(B_c \to D_s^*\left(\to D_s\pi\right)e^+e^-\right)_{[1.1,6.0]} = 0.614 \times 10^{-8},$$
$$\mathcal{B}\left(B_c \to D_s^*\left(\to D_s\pi\right)\mu^+\mu^-\right)_{[1.1,6.0]} = 0.616 \times 10^{-8},$$
$$\mathcal{B}\left(B_c \to D_s^*\left(\to D_s\pi\right)\tau^+\tau^-\right)_{[15.0,17.0]} = 0.087 \times 10^{-9}. \tag{33}$$

This quasi-fourfold distribution provides the number of angular observables to check for NP effects. So now we visit the NP models to trace out the NP. First of all, we here present the Wilson coefficients we used to trace out the NP, and separation between NP effects is based on the following shifts in values of Wilson coefficients and mainly the LFU NP contribution to C_{10}^{μ}; these are expressed as [78]:

$$C^{\mu}_{(9,10)} = C^{U}_{(9,10)} + C^{V}_{(9,10)},$$
$$C^{\tau}_{(9,10)} = C^{U}_{(9,10)}, \tag{34}$$

Table 3. The Wilson coefficients in different new scenarios [49].

Scenarios	Wilson coefficients	$1\,\sigma$ range	$\Delta\chi^2$
SI	C_9^U	-1.08 ± 0.18	27.90
SII	$C_9^U = -C_{10}^U$	-0.50 ± 0.12	18.85
SIII	$C_9^U = -C_{9'}^U$	-0.88 ± 0.16	26.92

Table 4. The Wilson coefficients in different new scenarios [49].

Scenarios	Wilson coefficients	1σ range	pull	Scenarios	Wilson coefficients	1σ range	pull
	$C_{9\mu}^V$	$[-1.31, -0.53]$	4.5	–	$C_{9\mu}^V = -C_{10\mu}^V$	$[-0.27, -0.12]$	3.6
SV	$C_9^U = C_{10}^U$	$[-0.13, 0.58]$	-	SIX	C_{10}^U	$[-0.09, 0.27]$	-
	$C_{10\mu}^V$	$[-0.66, 0.07]$	-	-	-	-	-
	$C_{9\mu}^V = -C_{10\mu}^V$	$[-0.33, -0.20]$	4.1	-	$C_{9\mu}^V$	$[-0.72, -0.41]$	4.6
SVI	$C_9^U = C_{10}^U$	$[-0.43, -0.17]$	-	SX	C_{10}^U	$[0.05, 0.34]$	-
	$C_{9\mu}^V$	$[-0.43, -0.08]$	5.5	-	$C_{9\mu}^V$	$[-0.82, -0.51]$	4.6
SVII	C_9^U	$[-1.07, -0.58]$	-	SXI	$C_{10'}^U$	$[-0.26, -0.04]$	-
	$C_{9\mu}^V = -C_{10\mu}^V$	$[-0.18, -0.05]$	5.6	-	$C_{9\mu}^V$	$[-0.96, -0.60]$	5.1
SVIII	C_9^U	$[-1.15, -0.77]$	-	SXII	$C_{9'\mu}^V$	$[0.22, 0.63]$	-
-	-	-	-	-	C_{10}^U	$[0.01, 0.38]$	-
-	-	-	-	-	$C_{10'}^U$	$[-0.08, 0.24]$	-

Table 5. Branching ratios in the bin $[1.1, 6.0]\,\mathrm{GeV}^2$ and $[15, 17]\,\mathrm{GeV}^2$ for the SM and different NP models.

$\mathcal{B}r\,(\mathrm{GeV}^{-2})$	$q^2\,(\mathrm{GeV}^2)$	SM (10^{-8})	SII(10^{-10})	SV(10^{-10})	SVI(10^{-10})
$\ell = e$	[1.1, 6.0]	0.614	[5.418, 4.532]	[4.730, 4.007]	[4.064, 4.686]
$\ell = \mu$	[1.1, 6.0]	0.616	-	[4.553, 8.901]	[4.267, 5.169]
$\ell = \tau$	[15, 17]	0.087	[0.107, 0.913]	[0.646, 0.729]	[0.749, 0.925]

where the Wilson coefficients $C_{(9,10)}^U$ are linked with the $b \to s\ell^+\ell^-$ $(\ell = e, \tau)$ and $C_{(9,10)}^V$ is associated with $b \to s\mu^+\mu^-$ [49]. LFU NP is allowed in particularly C_9^U as it was commonly held that these dropped out as the statistical point of view couldn't justify their presence. Still, their inclusion leads to a new paradigm. Vector couplings to muons are encoded in C_9^μ. LFU-violating NP affects only muons $C_{9e,\tau}^V = 0$. Scenario VIII containing universal coefficient coupling C_9^U together with the muonic part follows the $SU(2)_L$ invariance. These all are independent of external hadron states and their momentum-energy relations. Here we consider the values obtained from the complete data set and the three prominent $1D$ NP scenarios and eight $D > 1$ as presented in Tables 3 and 4.

Using the NP models mentioned in the above Tables 3 and 4, we assessed the physical observables in different q^2 bins and found significant deviations from the SM results. The calculated branching fractions for the quasi-four body process in the range $1.1\ \mathrm{GeV}^2 \leq q^2 \leq 6.0\ \mathrm{GeV}^2$ for the electron and muon and in the range $15\ \mathrm{GeV}^2 \leq q^2 \leq 17\ \mathrm{GeV}^2$ for tau are mentioned in

Table 6. Value of $R^{\tau e}$ in q^2 bin of [15, 17] GeV^2 in different scenarios.

[15, 17] GeV^2	SM	SII	SV	SVI
$R^{\tau e}$	0.3801	[0.0589, 0.6627]	[0.5790, 0.6748]	[0.6706, 0.6351]

Table 7. Results of $A_{\rm FB}$ in different q^2 bins for the three generations of leptons.

Observables	q^2 GeV^2	SM	SII	SV	SVI
$A_{\rm FB}\,(\ell = e)$	[1.1, 6.0]	−0.057	[−0.257, −0.175]	[−0.178, −0.062]	[0.081, 0.194]
	[6, 8]	−0.257	[−0.484, −0.300]	[0.029, 0.068]	[0.098, 0.347]
	[11, 12.5]	−0.381	[−0.463, −0.377]	[0.078, 0.148]	[0.194, 0.403]
	[15, 17]	−0.294	[−0.174, −0.113]	[−0.004, 0.036]	[0.049, 0.127]
$A_{\rm FB}\,(\ell = \mu)$	[1.1, 6.0]	−0.056	–	[−0.253, 0.244]	[−0.014, 0.044]
	[6, 8]	−0.256	–	[−0.125, 0.513]	[−0.003, 0.140]
	[11, 12.5]	−0.380	–	[−0.263, 0.393]	[−0.037, 0.098]
	[15, 17]	−0.294	–	[−0.121, 0.192]	[−0.009, 0.032]
$A_{\rm FB}\,(\ell = \tau)$	[1.1, 6.0]	0	0	0	0
	[6, 8]	0	0	0	0
	[11, 12.5]	0	0	0	0
	[15, 17]	−0.154	[−0.036, −0.056]	[−0.002, 0.010]	[0.014, 0.040]

Table 5 for all the relevant models. The mentioned scenarios exhibit significant deviations from the SM results, imprinting the NP effects.

Resonant particles, and charmonium states J/ψ and $\psi(2S)$ affect the widths greatly because of large dilepton masses and small widths, whereas those above the $D\bar{D}$ threshold due to their larger widths don't contribute effectively. Charmless vector mesons are suppressed by the factor λ_u.

We have investigated the physical observables, the lepton forward-backward asymmetry parameter, and the transverse and longitudinal polarization fractions. These observables (average value) are calculated by using the following equation:

$$\langle A \rangle = \frac{\int_{q^2_{\rm min}}^{q^2_{\rm max}} A\left[q^2\right]\left(\frac{d\Gamma}{dq^2} + \frac{d\bar{\Gamma}}{dq^2}\right) dq^2}{\int_{q^2_{\rm min}}^{q^2_{\rm max}} \left(\frac{d\Gamma}{dq^2} + \frac{d\bar{\Gamma}}{dq^2}\right) dq^2}. \tag{35}$$

Now we mention the numerical results of these observables, i.e. lepton forward-backward asymmetry and polarization fractions, in Tables 7 and 8 for the respective decay for all the relevant NP models in different q^2 bins and the impact of LFUV-NP and LFU NP can be observed as compared to SM results. It's clear from the results that R_K and R_{K^*} deviate from the corresponding ratios in the SM, signaling the presence of BSM theory. The q^2 dependence of these observables is represented in Figs. 2 and 3. The results depict the discrepancy between the results of NP and the SM with large deviations showing that $A_{\rm FB}$, F_L, and F_T are the best probes to search for BSM physics in different q^2 intervals for the specific scenarios mentioned in Table 4. Although no such measurements have been recorded experimentally, in the future, the LHCb can be expected to reveal the details of this quasi-four body decay to measure the corresponding observables. The ratios of branching fractions in different models deviate from 1 in the case of electron and muon, representing that electron and muon are different particles under the constraints of varying coupling strengths. Relative deviations of the observables of

Table 8. Results of F_L and F_T in different q^2 bins for the three generations of leptons.

Observables	q^2 (GeV^2)	SM	SII	SV	SVI
$\langle F_L\,(\ell=e)\rangle$	[1.1, 6.0]	0.870	[0.099, 0.052]	[0.431, 0.060]	[0.054, 0.058]
$\langle F_T\,(\ell=e)\rangle$	–	0.130	[0.901, 0.948]	[0.569, 0.940]	[0.946, 0.942]
$\langle F_L\,(\ell=e)\rangle$	[6, 8]	[0.719]	[0.433, 0.582]	[0.913, 0.805]	[0.773, 0.540]
$\langle F_T\,(\ell=e)\rangle$	–	0.281	[0.567, 0.418]	[0.087, 0.195]	[0.227, 0.460]
$\langle F_L\,(\ell=e)\rangle$	[11, 12.5]	0.535	[0.353, 0.331]	[0.635, 0.369]	[0.354, 0.334]
$\langle F_T\,(\ell=e)\rangle$	–	0.465	[0.647, 0.669]	[0.365, 0.631]	[0.646, 0.666]
$\langle F_L\,(\ell=e)\rangle$	[15, 17]	0.431	[0.401, 0.400]	[0.430, 0.404]	[0.403, 0.401]
$\langle F_T\,(\ell=e)\rangle$	–	0.569	[0.599, 0.600]	[0.570, 0.596]	[0.597, 0.599]
$\langle F_L\,(\ell=\mu)\rangle$	[1.1, 6.0]	0.867	–	[0.219, 0.218]	[0.012, 0.021]
$\langle F_T\,(\ell=\mu)\rangle$	–	0.133	–	–	–
$\langle F_L\,(\ell=\mu)\rangle$	[6, 8]	0.719	–	[0.822, 0.284]	[0.574, 0.146]
$\langle F_T\,(\ell=\mu)\rangle$	–	0.281	–	–	–
$\langle F_L\,(\ell=\mu)\rangle$	[11, 12.5]	0.536	–	[0.494, 0.383]	[0.286, 0.292]
$\langle F_T\,(\ell=\mu)\rangle$	–	0.464	–	–	–
$\langle F_L\,(\ell=\mu)\rangle$	[15, 17]	0.432	–	[0.412, 0.403]	[0.399, 0.398]
$\langle F_T\,(\ell=\mu)\rangle$	–	0.568	–	–	–
$\langle F_L\,(\ell=\tau)\rangle$	[1.1, 6]	–	–	–	–
$\langle F_T\,(\ell=\tau)\rangle$	–	–	–	–	–
$\langle F_L\,(\ell=\tau)\rangle$	[6, 8]	–	–	–	–
$\langle F_T\,(\ell=\tau)\rangle$	–	–	–	–	–
$\langle F_L\,(\ell=\tau)\rangle$	[11, 12.5]	–	–	–	–
$\langle F_T\,(\ell=\tau)\rangle$	–	–	–	–	–
$\langle F_L\,(\ell=\tau)\rangle$	[15, 17]	0.458	[0.381, 0.389]	[0.414, 0.383]	[0.382, 0.383]
$\langle F_T\,(\ell=\tau)\rangle$	–	0.542	[0.619, 0.611]	[0.586, 0.617]	[0.618, 0.617]

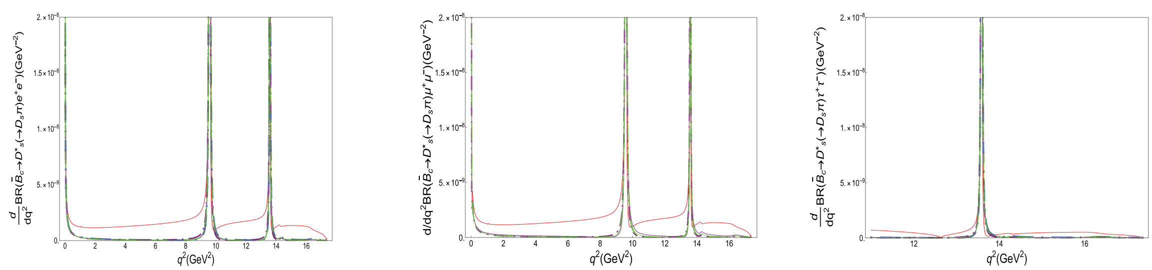

(a) (b) (c)

Fig. 2. The branching ratios of $B \to D_s^*(\to D\pi)\,\ell^+\ell^-$, for $\ell = e,\ \mu,\ \tau$ as a function of q^2 in the SM and various NP scenarios: SM (red solid line), SII upper interval (blue solid line), SII lower interval (blue dashed line), SV upper interval (purple solid line), SV lower interval (purple dashed line), SVI upper interval (green solid line), and SVI lower interval (green dashed line) of the Wilson coefficients.

the respective models from the SM are calculated. For example, we found a 91.9% deviation of the NP branching fraction from the SM value; for F_L, the relative deviation is 91.3%.

All the other relative deviations concerning SM results can be calculated easily. The CP-averaged coefficients $S_{1c(s)}$, $S_{2c(s)}$, and S_6 serve as the best probes to search for the BSM. The graphs in Fig. 3 depict variations of F_T, F_L, and $A_{\rm FB}$ with q^2 and Tables 7 and 8 present the results across different q^2 bins. In Fig. 3 and Tables 7 and 8, observables for the case $\ell = \mu$

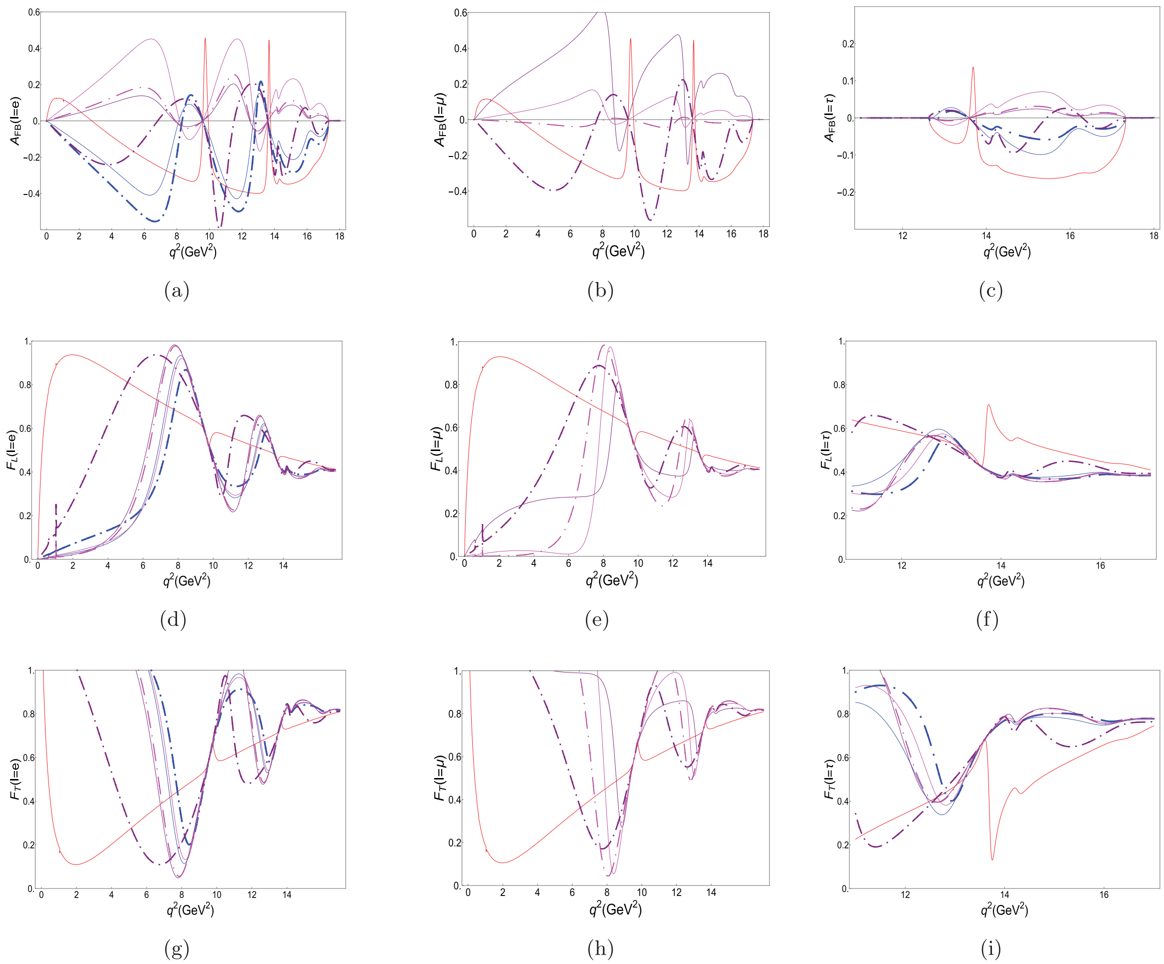

Fig. 3. The forward-backward asymmetry (a,b,c), and longitudinal (d, e, f) and transverse polarization (g, h, i) of $B \to D_s^* (\to D\pi)\, \ell^+\ell^-$, for $\ell = e,\ \mu,\ \tau$ as a function of q^2 in the SM and various NP scenarios: SM (red solid line), SII upper interval (blue solid line), SII lower interval (blue dashed line), SV upper interval (purple solid line), SV lower interval (purple dashed line), SVI upper interval (magenta solid line), and SVI lower interval (magenta dashed line) of the Wilson coefficients.

show some missing lines and data as compared to the other two leptons and the reason is that SII doesn't have $C^V_{9,10}$, as some models don't have all the $C^{U,V}_{9,10}$ to satisfy Eq. (34).

6. Summary

The rare semileptonic decays have shown some deviations from the SM results, motivating us to see if we can find some suitable way to interpret them. Using the latest measurements of $B_s \to \mu^+\mu^-$, $B_s \to \phi\mu^+\mu^-$, R_{K,K_S}, and R_{K^*} and adding the 254 observables, Algueró et al. [49] found the pattern of the NP that successfully explains the data. Here, we studied the effect of these new couplings on the angular profiles of the decay $B_c \to \left(D_s^* \to D\pi\right) \ell^+\ell^-$, where we have studied the fourfold distribution of this decay in detail and extracted the various possible physical observables from the different angular coefficients. Central values are taken for the form factors, so uncertainties associated with the form factors might show differences in the future if considered. Being exclusive decays, the initial and final state matrix elements are parametrized in terms of the form factors, which are nonperturbative quantities. We took the values of these form factors calculated in the covariant LFQM [48], where the cascade decays with the e and μ in the final state have been calculated with the branching ratio to be of the order of 10^{-8}. Due to the phase space suppression, for the τ case, the corresponding result is $\mathcal{O}\left(10^{-9}\right)$ in $q^2 \equiv [15, 17]$ GeV^2. When we used the NP Wilson coefficients from Ref. [49], this LFU ratio with τ to μ showed substantial deviations from the SM results. The case is the same for the other observables, i.e. the lepton forward-backward asymmetry and polarization asymmetries. Hence, these can serve as potential probes to search the NP. We hope that in the future, the experimental observations of these rare semileptonic decays at the LHCb and dedicated B-factories will help us to find suitable interpretations of these mismatches with the SM results.

Acknowledgements
We would like to thank Prof. M. Jamil Aslam for suggesting the project.

Funding

Open Access funding: SCOAP^3.

References

[1] S. Descotes-Genon, L. Hofer, J. Matias, and J. Virto, J. High Energy Phys. **06**, 092 (2016) [arXiv:1510.04239[hep-ph]] [Search inSPIRE].
[2] F. Beaujean, C. Bobeth, and D. van Dyk, Eur. Phys. J. C **74**, 2897 (2014) [arXiv:1310.2478[hep-ph]] [Search inSPIRE].
[3] G. Hiller and M. Schmaltz, Phys. Rev. D **90**, 054014 (2014) [arXiv:1408.1627[hep-ph]] [Search in SPIRE].
[4] P. Ball and R. Zwicky, Phys. Rev. D **71**, 014029 (2005) [arXiv:hep-ph/0412079] [Search inSPIRE].
[5] The LHCb Collaboration, J. High Energy Phys. **1307**, 084 (2013) [arXiv:1305.2168 [hep-ex]] [Search inSPIRE].
[6] The LHCb Collaboration, J. High Energy Phys. **09**, 179 (2015) [arXiv:1506.08777 [hep-ex]] [Search inSPIRE].
[7] S. Descotes-Genon, J. Matias, M. Ramon, and J. Virto, J. High Energy Phys. **01**, 048 (2013) [arXiv:1207.2753 [hep-ph]] [Search inSPIRE].
[8] S. Descotes-Genon, T. Hurth, J. Matias, and J. Virto, J. High Energy Phys. **05**, 137 (2013) [arXiv:1303.5794 [hep-ph]] [Search inSPIRE].
[9] The LHCb Collaboration, J. High Energy Phys. **08**, 055 (2017) [arXiv:1705.05802 [hep-ex]] [Search inSPIRE].
[10] R. Aaij et al. [LHCb Collaboration], Phys. Rev. Lett. **122**, 191801 (2019) [arXiv:1903.09252 [hep-ex]] [Search inSPIRE].
[11] LHCb Collaboration, Nature Phys. **18**, 277 (2022) [arXiv:2103.11769 [hep-ex]] [Search inSPIRE].
[12] R. Aaij et al. [LHCb Collaboration], Phys. Rev. Lett. **131**, 051803 (2023) [arXiv:2212.09152 [hep-ex]] [Search inSPIRE].
[13] R. Aaij et al. [LHCb Collaboration], Phys. Rev. D **108**, 032002 (2023) [arXiv:2212.09153 [hep-ex]] [Search inSPIRE].
[14] S. Ishaq, F. Munir, and I. Ahmed, J. High Energy Phys. **07**, 006 (2013).
[15] F. Munir, S. Ishaq, and I. Ahmed, Prog. Theor. Exp. Phys. **2016**, 013B02 (2016) [arXiv:1511.07075 [hep-ph]] [Search inSPIRE].
[16] Z. R. Huang, M. A. Paracha, I. Ahmed, and C. D. Lü, Phys. Rev. D **100**, 055038 (2019) [arXiv:1812.03491 [hep-ph]] [Search inSPIRE].
[17] A. Sikandar, M. J. Aslam, I. Ahmed, and S. Shafaq, Phys. Rev. D **100**, 056013 (2019) [arXiv:1909.04384 [hep-ph]] [Search inSPIRE].
[18] F. Munir Bhutta, Z. R. Huang, C. D. Lü, M. A. Paracha, and W. Wang, Nucl. Phys. B **979**, 115763 (2022) [arXiv:2009.03588 [hep-ph]] [Search inSPIRE].

[19] D. Das, B. Kindra, G. Kumar, and N. Mahajan, Phys. Rev. D **99**, 093012 (2019) [arXiv:1812.11803 [hep-ph]] [Search inSPIRE].

[20] M. K. Mohapatra and A. Giri, Phys. Rev. D **104**, 095012 (2021) [arXiv:2109.12382 [hep-ph]] [Search inSPIRE].

[21] A. Sikandar, M. J. Aslam, I. Ahmed, and S. Shafaq, J. Phys. G **49**, 105002 (2022).

[22] N. Rajeev, N. Sahoo, and R. Dutta, Phys. Rev. D **103**, 095007 (2021) [arXiv:2009.06213 [hep-ph]] [Search inSPIRE].

[23] R. Aaij et al. [LHCb Collaboration], Phys. Rev. Lett. **118**, 251802 (2017) [arXiv:1703.02508 [hep-ex]] [Search inSPIRE].

[24] V. S. Vobbilisetti, Search for $B^+ \to K^+\tau\tau$ with Belle and Belle (II) data samples. BELLE2-PTHESIS-2023-016 (Laboratoire de Physique des 2 Infinis Irène Joliot-Curie, Université Paris-Saclay, Orsay, 2023).

[25] S. Celani [LHCb], "Lepton Flavour Universality tests and Lepton Flavour Violation searches at LHCb,"[arXiv:2111.11105 [hep-ex]] [Search inSPIRE].

[26] T. V. Dong et al. [The Belle Collaboration], Phys. Rev. D **108**, L011102 (2023) [arXiv:2110.03871 [hep-ex]] [Search inSPIRE].

[27] L. Li and T. Liu, J. High Energy Phys. **06**, 064 (2021) [arXiv:2012.00665 [hep-ph]] [Search inSPIRE].

[28] A. K. Alok, N. R. S. Chundawat, J. Kumar, A. Mandal, and U. Tamponi, ["Genuine lepton-flavor-universality-violatingobservables in the $\tau - \mu$ sector of B → (K,K∗)ℓ+ℓ− decays," Phys. Rev. D **110** 055024, (2024). [arXiv:2405.18488 [ph-th]]. [Search inSPIRE].

[29] D. Bečirević, F. Jaffredo, J. P. Pinheiro, and O. Sumensari, Phys. Rev. D, **110**, 075004 (2024) arXiv:2407.19060 [hep-ph]] [Search inSPIRE].

[30] A. K. Alok, N. R. Singh Chundawat, and A. Mandal, Phys. Lett. B **847**, 138289 (2023) [arXiv:2303.16606 [hep-ph]] [Search inSPIRE].

[31] A. Ali, A. Y. Parkhomenko, and I. M. Parnova, Phys. Lett. B **842**, 137961 (2023) [arXiv:2303.15384 [hep-ph]] [Search inSPIRE].

[32] T. S. M. Ho, X. H. Jiang, T. H. Kwok, L. Li, and T. Liu, Phys. Rev. D **109**, 093004 (2024) [arXiv:2212.02433 [hep-ph]] [Search inSPIRE].

[33] P. Maji and S. Sahoo, Springer Proc. Phys. **261**, 875 (2021).

[34] C. Cornella, D. A. Faroughy, J. Fuentes-Martin, G. Isidori, and M. Neubert, J. High Energy Phys. **08**, 050 (2021) [arXiv:2103.16558 [hep-ph]] [Search inSPIRE].

[35] C. Cornella, G. Isidori, M. König, S. Liechti, P. Owen, and N. Serra, Eur. Phys. J. C **80**, 1095 (2020) [arXiv:2001.04470 [hep-ph]] [Search inSPIRE].

[36] T. Huber, T. Hurth, J. Jenkins, E. Lunghi, Q. Qin, and K. K. Vos, J. High Energy Phys. **10**, 088 (2020) [arXiv:2007.04191 [hep-ph]] [Search inSPIRE].

[37] The LHCb Collaboration, Eur. Phys. J. C **74**, 2839 (2014) [arXiv:1401.6932 [hep-ex]] [Search inSPIRE].

[38] R. Aaij et al. [LHCb Collaboration], Phys. Rev. Lett. **114**, 132001 (2015) [arXiv:1411.2943 [hep-ex]] [Search inSPIRE].

[39] LHCb Collaboration, Phys. Lett. B **742**, 29 (2015) [arXiv:1411.6899 [hep-ex]] [Search inSPIRE].

[40] LHCb Collaboration R. Aaij et al. [LHCb], JHEP02 **032**, (2024)[arXiv:2308.06162 [hep-ex]] [Search inSPIRE].

[41] C. Q. Geng, C. W. Hwang, and C. C. Liu, Phys. Rev. D **65**, 094037 (2002) [arXiv:hep-ph/0110376 [hep-ph]] [Search inSPIRE].

[42] W. F. Wang, X. Yu, C. D. Lü, and Z. J. Xiao, Phys. Rev. D **90**, 094018 (2014) [arXiv:1401.0391 [hep-ph]] [Search inSPIRE].

[43] V. V. Kiselev, Submitted on 4 Nov 2002 (v1), [arXiv:hep-ph/0211021] [hep-ph]] [Search inSPIRE].

[44] K. Azizi, F. Falahati, V. Bashiry, and S. M. Zebarjad, Phys. Rev. D **77**, 114024 (2008) [arXiv:0806.0583 [hep-ph]] [Search inSPIRE].

[45] R. Dutta, Phys. Rev. D **100**, 075025 (2019) [arXiv:1906.02412 [hep-ph]] [Search inSPIRE].

[46] M. K. Mohapatra, N. Rajeev, and R. Dutta, Phys. Rev. D **105**, 115022 (2022) [arXiv:2108.10106 [hep-ph]] [Search inSPIRE].

[47] M. Zaki, M. A. Paracha, and F. M. Bhutta, Nucl. Phys. B **992**, 116236 (2023) [arXiv:2303.01145 [hep-ph]] [Search inSPIRE].

[48] Y. S. Li and X. Liu, Phys. Rev. D **108**, 093005 (2023) [arXiv:2309.08191 [hep-ph]] [Search inSPIRE].
[49] M. Algueró, B. Capdevila, S. Descotes-Genon, J. Matias, and M. Novoa-Brunet, Eur. Phys. J. C **82**, 326 (2022) [arXiv:2104.08921 [hep-ph]] [Search inSPIRE].
[50] P. Bechtle, C. Chall et al. "Bottoms Up: Standard Model Effective Field Theory from a Model Perspective,"[arXiv:2201.08819 [physics.hist-ph]] [Search inSPIRE].
[51] G. Buchalla, A. J. Buras, and M. E. Lautenbacher, Rev. Mod. Phys. **68**, 1125 (1996) [arXiv:hep-ph/9512380] [Search inSPIRE].
[52] P. Colangelo, F. De Fazio, R. Ferrandes, and T. N. Pham, Phys. Rev. D **73**, 115006 (2006) [arXiv:hep-ph/0604029] [hep-ph][Search inSPIRE].
[53] S. P. Jin and Z. J. Xiao, Adv. High Energy Phys. **2021**, 3840623 (2021) [arXiv:2011.11409 [hep-ph]] [Search inSPIRE].
[54] M. J. Aslam, C. D. Lü, and Y. M. Wang, Phys. Rev. D **79**, 074007 (2009).
[55] J. Matias, F. Mescia, M. Ramon, and J. Virto, J. High Energy Phys. **1204**, 104 (2012) [arXiv:1202.4266 [hep-ph]] [Search inSPIRE].
[56] Particle Data Group, Prog. Theor. Exp. Phys. **2022**, 083C01 (2022).
[57] S. P. Jin, X. Q. Hu, and Z. J. Xiao, Phys. Rev. D **102**, 013001 (2020).
[58] N. R. Soni, A. Issadykov, A. N. Gadaria, J. J. Patel, and J. N. Pandya, Eur. Phys. J. A **58**, 39 (2022).
[59] W. F. Wang and Z. J. Xiao, Phys. Rev. D **79**, 074007 (2009) [arXiv:0902.0432 [hep-ph]] [Search in SPIRE].
[60] S.-P. Jin and Z.-J. Xiao, Adv. High Energy Phys. **2021**, 3840623 (2021) [arXiv:2011.11409 [hep-ph]] [Search inSPIRE].
[61] Particle Data Group, Prog. Theor. Exp. Phys. **2020**, 083C01 (2020).
[62] M. Wirbel, B. Stech, and M. Bauer, Z. Phys. C **29**, 637 (1985).
[63] P. Ball and V. M. Braun, Phys. Rev. D **58**, 094016 (1998) [arXiv:hep-ph/9805422] [Search inSPIRE].
[64] Z. Q. Zhang, Z. J. Sun, Y. C. Zhao, Y. Y. Yang, and Z. Y. Zhang, Eur. Phys. J. C **83**, 477 (2023) [arXiv:2301.11107 [hep-ph]] [Search inSPIRE].
[65] W. Jaus, Phys. Rev. D **60**, 054026 (1999) [arXiv:1103.2973 [hep-ph]] [Search inSPIRE].
[66] H. Y. Cheng, C. K. Chua, and C. W. Hwang, Phys. Rev. D **69**, 074025 (2004) [arXiv:hep-ph/0310359] [Search inSPIRE].
[67] A. Faessler, Th. Gutsche, M. A. Ivanov, J. G. Körner, and V. E. Lyubovitskij, Eur. Phys. J. Direct **18**, C4 (2002) [arXiv:hep-ph/0205287] [Search inSPIRE].
[68] W. Altmannshofer, P. Ball, A. Bharucha, A. J. Buras, D. M. Straub, and M. Wick, J. High Energy Phys. **01**, 019 (2009) [arXiv:0811.1214 [hep-ph]] [Search inSPIRE].
[69] D. Becirevic and E. Schneider, Nucl. Phys. B **854**, 321 (2012) [arXiv:1106.3283 [hep-ph]] [Search inSPIRE].
[70] H.-Y. Cheng and X.-W. Kang, Eur. Phys. J. C **77**, 587 (2017).
[71] Q. Chang, L. T. Wang, and X. N. Li, J. High Energy Phys. **12**, 102 (2019).
[72] K. Chen, H. W. Ke, X. Liu, and T. Matsuki, Chin. Phys. C **43**, 023106 (2019) [arXiv:1707.02523 [hep-ph]][Search inSPIRE].
[73] Y. M. Wang, Y. B. Wei, Y. L. Shen, and C. D. Lü, J. High Energy Phys. **1706**, 062 (2017).
[74] V. V. Kiselev,, [Submitted on 21 Aug 2003, [arXiv:hep-ph/0308214].] [Search inSPIRE].
[75] X.-J. Li, Y.-S. Li, F.-L. Wang, and X. Liu, "Spectroscopic survey of higherlyingstates of Bc meson family," Eur. Phys. J. C, **83**, 1080 (2023). [arXiv:2308.07206 [hep-ph]] [Search inSPIRE].
[76] W. Wang, Y. L. Shen, and C. D. Lu, Phys. Rev. D **79**, 054012 (2009) [arXiv:0811.3748 [hep-ph]] [Search inSPIRE].
[77] K. De Bruyn, R. Fleischer, E. Malami, and P. van Vliet, J. Phys. G Nucl. Part. Phys. **8**, 054012 (2022) [arXiv:2208.14910[hep-ph]] [Search inSPIRE].
[78] A. Bharucha, D. M. Straub, and R. Zwicky, J. High Energy Phys. **08**, 098 (2016) [arXiv:1503.05534 [hep-ph]] [Search inSPIRE].

Funded by SCOAP[3]